Analysis of Lung Surfactant Model Systems with Time-of-Flight Secondary Ion Mass Spectrometry

Nikolaus Bourdos,* Felix Kollmer,† Alfred Benninghoven,† Michaela Ross,* Manfred Sieber,* and Hans-Joachim Galla*

*Institut für Biochemie and †Physikalisches Institut, Westfälische Wilhelms-Universität, D-48149 Münster, Germany

ABSTRACT An often-used model lung surfactant containing dipalmitoylphosphatidylcholine (DPPC), dipalmitoylphosphatidylglycerol (DPPG), and the surfactant protein C (SP-C) was analyzed as Langmuir-Blodgett film by spatially resolved time-of-flight secondary ion mass spectrometry (TOF-SIMS) to directly visualize the formation and composition of domains. Binary lipid and lipid/SP-C systems were probed for comparison. TOF-SIMS spectra revealed positive secondary ions (SI) characteristic for DPPC and SP-C, but not for DPPG. SI mapping results in images with domain structures in DPPC/DPPG and DPPG/SP-C, but not in DPPC/SP-C films. We are able to distinguish between the fluid and condensed areas probably due to a matrix effect. These findings correspond with other imaging techniques, fluorescence light microscopy (FLM), scanning force microscopy (SFM), and silver decoration. The ternary mixture DPPC/DPPG/SP-C transferred from the collapse region exhibited SP-C-rich domains surrounding pure lipid areas. The results obtained are in full accordance with our earlier SFM picture of layered protrusions that serve as a compressed reservoir for surfactant material during expansion. Our study demonstrates once more that SP-C plays a unique role in the respiration process.

INTRODUCTION

The lung surfactant is a complex mixture of lipids, proteins, and carbohydrates (Harwood, 1987; King and Clements, 1972; Shelly et al., 1984) lining out the hypophase of the alveolar epithelium and maintaining lung stability by reducing the surface retractive force. The surface tension was reported to be very small in vivo (Schürch et al., 1976) or even zero (Cochrane and Revak, 1991). According to the surfactant monolayer theory (Clements, 1962) this is attained by almost pure monolayers of dipalmitoylphosphatidylcholine (DPPC) (Bangham, 1979), where non-DPPC components are supposed to be squeezed out from the monolayer at compression/exhalation and respread into the monolayer at expansion/inhalation. This theory, however, is questioned by Scarpelli and Mautone (1994), stating that it is incompatible with regional lung function.

Four lung surfactant proteins (SP) are known: the hydrophilic SP-A and SP-D, and the hydrophobic SP-B and SP-C (Johansson et al., 1994a, Johansson and Curstedt, 1997). SP-C is a small amphipathic peptide of 33 to 35 amino acid residues depending on the species, with a large α-helical portion composed mainly of valine and leucine residues, making it extremely hydrophobic (Johansson et al., 1994b). The flexible and disordered amino terminal domain includes two palmitoyl residues in the human peptide. SP-B and SP-C are probably responsible for many of the surface properties of the lung surfactant, such as promoting the insertion of phospholipids into monolayers and enabling the adsorption of surfactant material from vesicles to the air/water interface or to a preexisting monolayer (Oosterlaken-Dijksterhuis et al., 1991a, b; Pèrez-Gil et al., 1992b; Wang et al., 1995, 1996a, b). In film balance measurements on mixed phospholipid films with SP-B and SP-C, exclusion of proteins or proteins associated with phospholipids from the monolayer was found (Taneva and Keough, 1994a–d). This exclusion is obviously accomplished by formation of multilayer structures, either observed directly with imaging techniques or derived from other measurements (Amrein et al., 1997; Galla et al., 1998; Liu, 1997; Post et al., 1995; Schürch et al., 1995; Sen et al., 1988; Tchoreloff et al., 1991; von Nahmen et al., 1997a, b). It is reported that the excluded material remains adsorbed to the monolayer as multilayer stacks representing a reservoir from which the excluded material becomes reinserted into the monolayer upon expansion. A complete reinsertion of excluded material is already accomplished by SP-C alone, as was shown in a compression/expansion cycle for a mixture of DPPC, dipalmitoylphosphatidylglycerol (DPPG), and SP-C (Galla et al., 1998).

Multilayer stacks in such a film are formed when the isotherm turns into the plateau region at $\approx$50 mN/m (see Fig. 1). In our laboratory their existence and the topology were derived by ellipsometry (Post et al., 1995), from the intensity distribution in fluorescence micrographs (von Nahmen et al., 1997b), and by scanning force microscopy (SFM) (Amrein et al., 1997; von Nahmen et al., 1997a). Protrusions have also been found recently in a surfactant film containing SP-B and SP-C, but far below the plateau point (Krüger et al., 1999). Although highly valuable to visualize lateral domain formation in surfactant model systems, neither fluorescence light microscopy (FLM) (Discher et al., 1996; Horowitz et al., 1992; Pèrez-Gil et al., 1992a; Nag et al., 1996, 1997; von Nahmen et al., 1997b) nor SFM

Received for publication 5 November 1999 and in final form 29 March 2000.

Address reprint requests to Hans-Joachim Galla, Institut für Biochemie, Wilhelm-Klemm-Strasse 2, Westfälische Wilhelms-Universität, D-48149 Münster, Germany. Tel.: +49-251-8333201; Fax: +49-251-8333206; E-mail: gallah@uni-muenster.de.

0006-3495/00/07/357/13 $2.00

(Amrein et al., 1997; Panaiotov et al., 1996; von Nahmen et al., 1997a) are able to yield laterally resolved chemical information, because normal SFM imaging is caused by a topography-modulated signal, whereas FLM contrast depends on the lateral distribution of a dye, determined by its lipid solubility.

In this study, time-of-flight secondary ion mass spectrometry (TOF-SIMS) is used to visualize and chemically analyze the domain formation in solid-supported Langmuir-Blodgett films consisting of DPPC, DPPG, and SP-C. The sample ("target") is probed by a primary ion (PI) beam, which induces a collision cascade among the target atoms (Benninghoven et al., 1993; Benninghoven, 1994), which again causes the desorption of atoms, molecules, or quasi-molecules, and molecular fragments out of the uppermost layers of the target. Only 1% of the sputtered secondary particles are ions. The mass of these secondary ions (SI) is calculated in a TOF analyzer. TOF analyzers attain low detection limits (a few femtomoles) and allow quasi-simultaneous mass detection with no theoretical upper limit. Actually, this limit is given by the desorption process; it was found to be 15,000 atomic mass units (amu) for polymers and 3500 amu for peptides so far (Hagenhoff, 1995). Nevertheless, TOF-SIMS spectra are mainly characterized by distinct fragmentation up to ≈500 amu, the so-called fingerprint regime. Fingerprint SI are utilized for identification of large molecules that lie beyond the detection limit, or in case of lacking desorption as molecular or quasi-molecular ion. The formation of quasi-molecular ions arises, considering the positive ion mode only, from protonation of the intact molecule, $(M + H)^+$, cationization by alkaline metals, e.g., sodiation $(M + Na)^+$, or substrate atoms, e.g., gold $(M + Au)^+$.

If a TOF-SIMS device is equipped with a sharply focused PI beam and scanning optics, it can be used for imaging a surface (see Materials and Methods). The measurement is then no longer restricted to mere identification of a compound but permits the determination of its lateral distribution in the uppermost layers of a sample. Because the intensity of an SI depends in a complex correlation from the environment, in which its parental molecule is embedded, it is complicated to quantify the local surface concentration of a molecule. However, this so-called *matrix effect* allows visualization of co-existing phases in LB layers (Leufgen et al., 1996; Bourdos et al., 2000), taking advantage of the different SI flux in both the liquid-expanded and the condensed phase, respectively. Other TOF-SIMS investigations on solid-supported LB films included stearic acid, self-assembled monolayers of thiols, polymethylacrylate, and gramicidin, (Hagenhoff et al., 1993; Hagenhoff, 1995). Further applications are given by Bertrand and Weng (1996).

The aim of this study is to analyze the composition of domain structures in films consisting of the two major surfactant phospholipid components DPPC and DPPG, and their mixtures with SP-C, by TOF-SIMS. The collapsed ternary film is of particular interest, because protrusions with only indirectly characterized chemical composition were observed after compression, which might explain the mechanism behind compression-expansion behavior of the alveolar surfactant upon breathing.

MATERIALS AND METHODS

Materials

1,2-Dipalmitoyl-*sn*-glycero-3-phosphocholine (DPPC), 1,2-dipalmitoyl-*sn*-glycero-3-(phospho-*rac*-(1-glycerol)) (DPPG), 1-palmitoyl-2-(6-((7-*nitro*-2-1,3-benzoxadiazol-4-yl)amino)caproyl)-*sn*-glycero-3-phosphocholine (NBD-PC), and 1-palmitoyl-2-(6-((7-*nitro*-2-1,3-benzoxa-diazol-4-yl)amino)-caproyl)-*sn*-glycero-3-(phospho-*rac*-(1-glycerol)) (NBD-PG) were purchased from Avanti Polar Lipids, Inc. (Alabaster, AL) and used without further purification. Chloroform and methanol were obtained from Sigma, *n*-hexane from Fluka (both Deisenhofen, Germany). All solvents were HPLC grade.

A dipalmitoylated form of the human recombinant surfactant protein C with the sequence Gly-Ile-Pro-Cys-Cys-Pro-Val-His-Leu-lys-Arg-Leu-Leu-Ile-Val-Val-Val-Val-Val-Val-Leu-Ile-Val-Val-Val-Ile-Val-Gly-Ala-Leu-Leu-Met-Gly-Leu was supplied generously by Byk-Gulden Pharmaceuticals (Konstanz, Germany), where the two cysteins are palmitoylated.

Tempax glass slides, 25 × 11 × 1.1 mm, were purchased from Rettberg (Göttingen, Germany). Gold (purity > 99.999%) was supplied generously by Degussa (Hanau, Germany).

FLM at the air/water interface

The fluorescence micrograph of DPPC/DPPG (molar ratio 4:1) containing 0.4 mol % SP-C and 1 mol % NBD-PC was obtained with the setup described in von Nahmen et al. (1997b) using an analog video recorder. The DPPG/SP-C film (0.5 mol % SP-C, plus 1 mol % NBD-PG) was visualized using a full digital setup. We used a CCD camera, whose signal is fed into a frame grabber card (both Hamamatsu, Herrsching, Germany) and displayed on a PC monitor. With this setup we obtained much better contrast and the micrographs were less noisy than with the analog equipment. The film compression rate was 1.9 $Å^2 \times \text{molecule}^{-1} \times \text{min}^{-1}$.

Preparation of gold-covered glass slides

The glass slides were cleaned by bath sonication at 70°C, alternately in detergent and water, three times in each case. The water was purified using a Milli-Q_{185} Plus system (Millipore GmbH, Eschborn, Germany). Immediately before evaporation the slides were dried in a nitrogen stream and further treated with argon plasma. First, 1 nm of chromium was deposited on the surface of the slide, serving as an adhesive layer, onto which 200 nm of gold were evaporated at a rate of 0.01 nm/s. The gold-covered slides were rectified 8 h in a Soxhlet using *n*-hexane.

Film deposition

The films were prepared by spreading chloroform/methanol (1:1, v/v) solutions of lipid/SP-C mixtures on a pure water subphase in a Teflon trough (FW2, maximal interfacial area 927 cm^2, Lauda-Königshofen, Germany) at a temperature of 20 ± 1°C. Binary lipid/protein mixtures were prepared with a 0.5 mol % SP-C content. A DPPC/DPPG mixture was prepared at a 4:1 molar ratio without SP-C and with a content of 0.4 mol % SP-C, respectively. After solvent evaporation (10–15 min) the films were equilibrated to a prespecified pressure (±1 mN/m). The gold-covered glass slides were again treated with argon plasma and immersed with a film lift vertically into the subphase at 300 mm/min; after 5 min the slide was drawn out. Deposition at pressures below the collapse was performed in a constant-pressure mode, where the speed of the film lift of 2 mm/min was

used and the barrier speed is accommodated to it, thus keeping lateral pressure constant during transfer. To transfer the collapsed state, the compression speed was accommodated to the speed of the film lift.

Silver decoration (SD)

According to Gleiche et al. (1998), a DPPC/DPPG film was prepared at 6 mN/m as described above, but deposited on mica (Electron Microscopy Science, Munich, Germany). A thin overlayer of silver (3.5 nm) was evaporated onto the lipid film to obtain optical contrast between the fluid and condensed domains. The samples were viewed with a conventional light microscope, digital images were acquired by a CCD camera connected to a frame grabber card in a PC.

TOF-SIMS measurements

The samples were placed in a vacuum chamber at pressures $< 10^{-8}$ torr. The device was equipped with a pulsed gallium PI source, with an ion energy of 30 keV (4.8×10^{-13} J), and a TOF analyzer of the reflectron type. This setup has been described in detail elsewhere (Schwieters et al., 1991) and was used earlier to study LB films of phospholipids (Leufgen et al., 1996; Bourdos et al., 2000). In the present modified form a grid-less reflectron was used, which accounts for enhanced SI yields due to higher transmission, and improved mass resolution (Kollmer, unpublished observations). While scanning a certain area by the PI beam, a spectrum was acquired at each pixel of the digital raster. For a given SI one thus obtains a map of its lateral distribution by assigning its intensity at a pixel to a value of a gray scale or color map, a procedure termed *molecular mapping*. In principle, the Ga^+ beam could be focused to a spot diameter of ≈80 nm. However, in our experiments a lateral resolution of 0.5 to 1 μm was obtained, corresponding to scan areas of 60×60 and 120×120 μm^2, respectively, in a 128×128 raster (for a better understanding of the factors determining lateral resolution see, for example, Kötter and Benninghoven, 1998; Rulle, 1996). In this study we mainly mapped positive ions. A mass spectrum was obtained by integrating SI intensities over the entire scan area. To achieve high mass resolution, the PI pulse was *bunched*, which means that a 15-nm pulse of Ga^+ ions was compressed "temporally" to ≈1 nm by time-dependent acceleration. Because the moment of the PI impact must be well-defined to serve as zero-setpoint for the time-of-flight measurement, short pulses enhance mass resolution. A disadvantage is the spatial spread of the PI beam due to Heisenberg's uncertainty relation, resulting in a defocused beam, which was unsuitable for imaging. As a consequence, imaging had to be carried out without bunching; thus the mapping of many SI was afflicted with interference between adjacent peaks due to low mass resolution, for example CH_4N^+ and $^{13}CCH_5^+$, both of which have the nominal mass of 30 amu (CH_4N^+ is typical of peptides, whereas the latter is an isotopomer of the unspecific $C_2H_5^+$). This became obvious as the mass resolution of the TOF-SIMS device was greatly enhanced over the recent years. However, because the larger SI are less intense, the two DPPC quasi-molecules $(DPPC \pm H)^+$ along with their isotope clusters were mapped as sum instead of a single peak to get an image with sufficient brightness. Except for the atomic ions like Ca^+, a fragment will be termed "M" together with the nominal mass, so instead of $C_4H_{10}N^+$ we use the term M72. We do not use the mass-to-charge ratio m/z because the SI are all singly charged.

RESULTS

Surface pressure-area diagram

Fig. 1 shows the surface pressure-area diagram of the ternary model system, containing DPPC, DPPG, and SP-C, which is a commonly used mixture to mimic the alveolar lung surfactant (von Nahmen et al., 1997a, b). Here we only focus on the prominent plateau formed at an average molecular area of ≈0.45 nm^2. According to earlier results, material is excluded from the monolayer upon further compression because the area where the plateau formation starts corresponds to the minimal area that can be occupied by the molecules being exclusively at the surface (without SP-C the collapse area is ≈0.42 nm^2). The excluded material constitutes a multilamellar phase, whose distinct topography was characterized by SFM in supported LB layers. In this model SP-C is thought to stabilize the multilamellar stacks (von Nahmen et al., 1997a). Intensity distribution measurements of the fluorescence at the air/water interface strongly support the idea of three-dimensional structures formed upon film collapse (von Nahmen et al., 1997b).

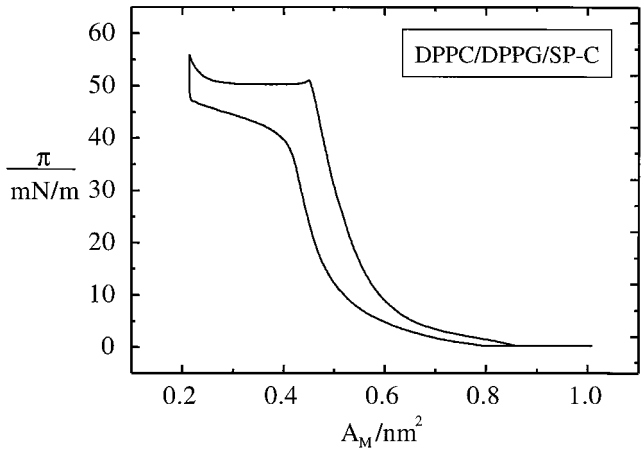

FIGURE 1 Surface pressure-area diagram of a monolayer of DPPC, DPPG, and SP-C on a pure water subphase at pH 5.8 and at 20°C. The molar ratio of DPPC and DPPG is 4:1, the SP-C content is 0.4 mol %. The isotherm exhibits an extensive plateau region close to 50 mN/m. Cyclic compression beyond the plateau always develops the same isotherm; the film collapse is fully reversible.

Mass spectra of SP-C and DPPC/DPPG/SP-C

Figs. 2 and 3 show TOF-SIMS spectra of positive SI of DPPC/DPPG/SP-C films deposited in the plateau region, and SP-C alone, respectively. From the latter, only the fingerprint range below 150 amu is shown, with a distinct fragmentation. A spectrum of pure DPPC was shown elsewhere (Bourdos et al., 2000). The primary ion dose density (PIDD) is given for the mass spectra and SI images, which is the PI number (or PI dose) per cm^2, applied during the measurement of the respective sample.

The spectrum of our model lung surfactant (Fig. 2) contains intense fingerprint fragments like M58, M70, M72, M86, M104, M125, M150, M166, M184, and M224, each of which originates from DPPC and/or SP-C (see Table 1) with a mass resolution as high as $m/\Delta m \approx 14{,}000$ for M41, where Δm is the full-width at half-maximum. M184 repre-

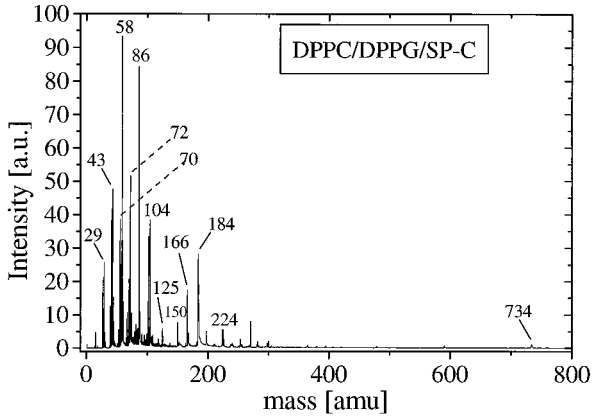

FIGURE 2 TOF-SIMS spectrum of positive SI from an LB layer of DPPC/DPPG/SP-C, prepared at plateau pressure on gold. PIDD: 3.4 × 10^{12} cm^{-2}.

sents the entire polar headgroup of DPPC (phosphocholine residue), whereas M224 results from the cleavage of both palmitoyl residues. DPPG does not yield any specific positive fragment except the protonated phosphoglycerol residue M173, but with a much lower intensity compared to the DPPC headgroup fragment M184. In the molecular ion region, one obtains the molecular ion (DPPC ± H)$^+$ (M732.5 and M734.5) and their isotope pattern. The DPPG quasi-molecular ion can only be observed in the negative SI spectrum of the ternary film (spectrum not shown, but the yield of DPPG$^-$ is given in Table 1).

The SP-C spectrum (Fig. 3) includes several distinct fingerprint fragments M18, M30, M44, M70, M72, M86, and M110. M4024 represents the molecular ion (SP-C + H)$^+$, which does not desorb from the mixed LB layer. Some fragments interfere with those obtained from DPPC, as M72 and M86, but others (M18, M30, M110) are SP-C-specific here. In both the phospholipid spectra and the SP-C spectrum, the region below 100 amu is largely populated by hydrocarbon SI, for example M15, M27, or M55. They originate mainly from each of the three compounds but to a small extent represent impurities found on a pure gold surface as well. An analysis of the single compounds showed that calcium ions originate primarily from the DPPG. Because no calcium ions were added to the lipid preparation and DPPG is purchased as sodium salt, it must be considered as an "impurity."

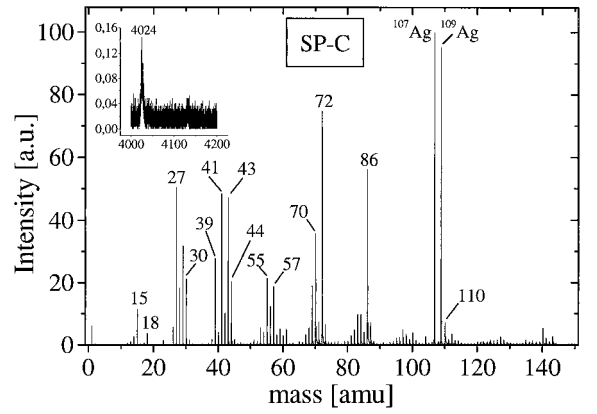

FIGURE 3 TOF-SIMS spectrum (fingerprint range) of positive SI from SP-C, prepared on silver by spin-coating of 1 nmol of SP-C, solved in isopropanol/water. PIDD: 6.8 × 10^{11} cm^{-2}. *Inset:* molecular ion peak of SP-C.

TABLE 1 SI obtained from the lung surfactant components DPPC, DPPG, and SP-C, used in this study as a surface active material that is thought to mimic the alveolar lung surfactant

m/z (amu)	Ion	DPPC	DPPG	SP-C	*Y(X)*/10^6
15	CH_3^+	+	+	+	200
18	NH_4^+	—	—	+	25
26	CN^-	+	−	+	120
27	$C_2H_3^+$	+	+	+	870
30	CH_4N^+	−	−	+	150
39	$C_3H_3^+$	+	+	+	480
40	Ca^+	+	+	+	70
41	$C_3H_5^+$	+	+	+	1700
42	CNO^-	+	−	+	70
43	$C_3H_7^+$	+	+	+	1600
44	$C_2H_6N^+$	−	−	+	480
55	$C_4H_7^+$	+	+	+	1200
57	$C_4H_9^+$	+	+	+	7900
58	$C_3H_8N^+$	+	−	+	4900
59	$C_3H_9N^+$	+	−	+	1400
70	$C_4H_8N^+$	+	—	+	790
72	$C_4H_{10}N^+$	+	−	+	2400
86	$C_5H_{12}N^+$	+	−	+	4600
102	$C_5H_{12}NO^+$	+	−	−	1400
104	$C_5H_{14}NO^+$	+	−	−	1600
110	$C_5H_8N_3^+$	−	−	+	40
125	$C_2H_6PO_4^+$	+	−	−	180
150	$C_5H_{13}NPO_2^+$	+	−	−	300
166	$C_5H_{13}NPO_3^+$	+	−	−	700
173	$C_3H_{10}PO_6^+$	−	+	−	6
184	$C_5H_{15}NPO_4^+$	+	−	−	2000
197	Au^+	−	−	−	180
224	$C_8H_{19}NPO_4^+$	+	−	−	200
225	$AuC_2H_4^+$	+	+	+	170
722	$DPPG^-$	−	+	−	6
735	$(DPPC+H)^+$	+	−	−	40
767*	$(DPPG+2Na-H)^+$	−	+	−	0.5
4024*	$(SP\text{-}C+H)^+$	−	−	+	2

Many of the SI are hydrocarbon ions, which are unspecific and have no relevance for identification purposes. Note that there is no prominent fingerprint SI from DPPG except $C_3H_{10}PO_6^+$. DPPC yields some intense polar headgroup fragments, such as M86, M104, M150, M166, M184, or M224. Their molecular structures are given elsewhere (Ayanoglu et al., 1984). The SI yields are related to the spectrum of the positive SI from the ternary LB film in the plateau, except the yield of CN^-, CNO^-, and $DPPG^-$, determined in the negative ion mode. Yields of ions marked by an asterisk are calculated from the respective single compound spectrum. The yield *Y(X)* of an SI *X* is determined by

$$Y(X) = \frac{\text{number of detected secondary ions } X}{\text{number of primary ions}}.$$

The most prominent SI and their yields are summarized in Table 1; the yields are calculated from films prepared in the plateau region. Although we do not show negative spectra here because of their very few specific fragments, it should be mentioned that DPPG is detected as entirely negative SI in both the single compound and the ternary film. The most prominent negative fingerprint fragments, originating from both DPPC and SP-C, are M26 (CN^-) and M42 (CNO^-). Their yields given in the table are calculated from the spectrum of the ternary mixture, in the single compound spectra one obtains much higher yields (Bourdes, unpublished results): for M26, e.g., $Y = 3000 \cdot 10^{-6}$ from SP-C and $Y = 1100 \cdot 10^{-6}$ for M26 from DPPC, for M42 we got $Y = 1800 \cdot 10^{-6}$ from SP-C and $170 \cdot 10^{-6}$ from DPPC, respectively. Because the yield of M42 resulting from SP-C is 10-fold larger than from DPPC, we expect a clear contrast in the image of mixed films containing SP-C. From DPPG the yields of M26 and M42 are negligible.

Binary films

Images of positive SI of DPPC/DPPG monolayers at 6 and 30 mN/m are given in Fig. 4, *A–H*, together with a sum image of diverse positive SI (Fig. 4 *I*) and a Ca^+ map (Fig. 4 *K*). A light-microscopic image of a silver-decorated sample (Fig. 4 *L*) is given for comparison. At 6 mN/m phase separation is imaged by the DPPC headgroup fragments (Fig. 4, *C* and *E*) and the molecular ion (Fig. 4 *G*) which is also true for the hydrocarbon ion M27 (Fig. 4 *A*) and Ca^+ (Fig. 4 *K*) which, however, exhibits an inverse contrast compared to the headgroup SI. The silver decoration image strongly resembles the TOF-SIMS images. At 30 mN/m no domains are observed (Fig. 4, *B*, *D*, *F*, and *H*), each of the SI is desorbed homogeneously, denoting no or not distinctly enough separated phases to be discriminated.

DPPC/SP-C films were prepared again at 6 and 30 mN/m (Fig. 5), DPPG/SP-C films at 6, 30, and 50 mN/m (Fig. 6); both were analyzed with TOF-SIMS and FLM. FLM-pictures of DPPC/SP-C films have been published before (von Nahmen, 1997). In addition, an SFM image of DPPG/SP-C in the plateau is presented in Fig. 6 *M*. The isotherms of both mixtures exhibit plateau regions at ≈50 mN/m, but the DPPC/SP-C film could not be transferred due to a continuous pressure drop. At 6 and 30 mN/m no domains are observed in DPPC/SP-C for either a DPPC-specific (M58, Fig. 5, *A* and *B*) or SP-C-specific SI (M110, Fig. 5, *C* and *D*). The DPPG/SP-C film maintained a stable equilibrium pressure in the plateau region when the compression was halted before transferring the film. Several SI distributions make domains at each pressure, three of them are shown as an example in Fig. 6: the contrast of the distributions of the hydrocarbon ion M27 (Fig. 6, *A–C*) and Ca^+ (Fig. 6 *L*, only shown for the plateau region) is found to be inverse to that of the amino acid fragments M72 and M86 (Fig. 6, *D–F* and

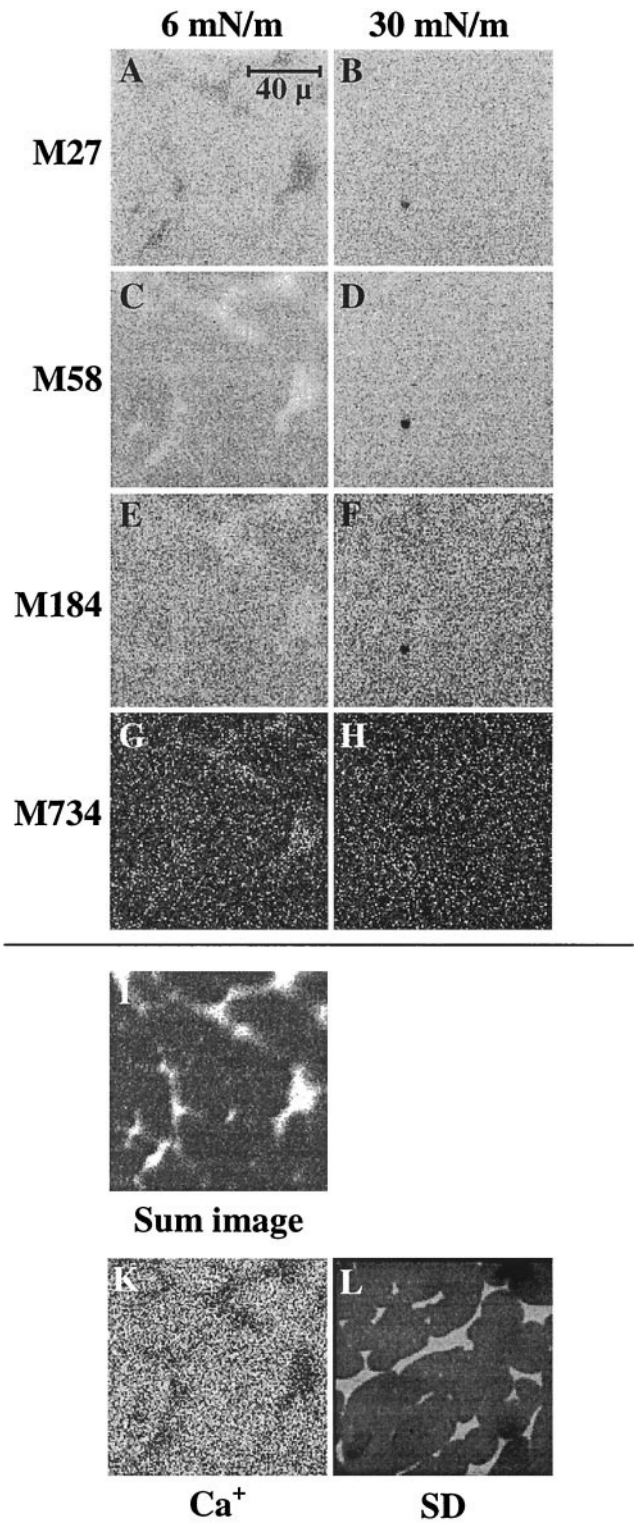

FIGURE 4 Images of DPPC/DPPG monolayers. (*A–H*) Maps of positive SI at 6 and 30 mN/m. PIDD: 1.0×10^{13} cm^{-2} (6 mN/m), 7.0×10^{12} cm^{-2} (30 mN/m); (*I*) 6 mN/m, Ca^+; (*K*) 6 mN/m, sum image of several positive SI; (*L*) 6 mN/m, silver-decorated; (*I*) and (*K*) are digitally enhanced.

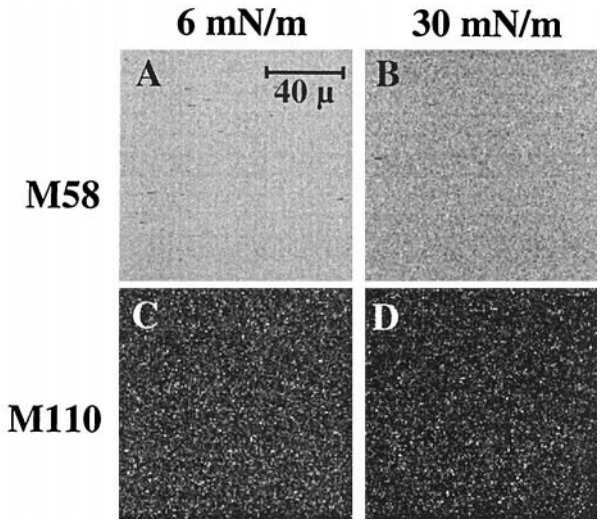

FIGURE 5 Images of DPPC/SP-C monolayers. Maps of positive SI at 6 and 30 mN/m. PIDD: 7.4 × 10^{12} cm^{-2} (6 mN/m), 4.9 × 10^{12} cm^{-2} (30 mN/m).

G–I). Mapping of M86 yields discernable contrast at low pressure (Fig. 6 *G*), although the total intensity over the entire scan area is low, at high pressure (Fig. 6, *H* and *I*) the SI distribution is more homogeneous. FLM reveals that during compression the domain size and structure do not change substantially (Fig. 6, *N–P*). At 30 mN/m (Fig. 6 *O*) a large portion of the film is still fluid (bright areas), although domains have become slightly smaller, and in the plateau region (Fig. 6 *P*) fluid domains get even brighter, which is, however, not observed in the ion images of the amino acid SI (Fig. 6, *F* and *I*). The domain shapes of the fluorescence micrograph at 6 mN/m (Fig. 6 *N*) correspond well to the related SI images (Fig. 6, *D* and *G*), whereas they differ somewhat at 30 mN/m (TOF-SIMS: Fig. 6, *E* and *H*; FLM: Fig. 6 *O*) and in the plateau (TOF-SIMS: Fig. 6, *F* and *I*; FLM: Fig. 6 *P*). Decreasing contrast at high pressures makes comparison of the different methods more difficult. However, the fluorescence image of the plateau (Fig. 6 *P*) closely resembles the scanning force micrograph (Fig. 6 *M*), in which the bright areas indicate elevated height. To obtain a better-contrasted SI image we summed up SP-C-specific SI distributions (Fig. 6 *K*). This illustrates that results obtained with TOF-SIMS, FLM, and SFM are quite similar.

Ternary DPPC/DPPG/SP-C film

Films were prepared and investigated at 6, 30, and 50 mN/m (plateau). In the positive ion mode, and similar to the DPPC/DPPG film, domains are observed at 6 mN/m and in the collapsed film, but not at 30 mN/m. At 6 mN/m, the mapping of M27, M70, M104, M110, M734 (Fig. 7, *A*, *D*, *G*, *K*, and *Q*) and other SI (e.g., Ca^+) yields distinct domain structure, with inverted distributions of M27 and M104. M184 is distributed more homogeneously, but still exhibits an observable contrast (Fig. 7 *N*). M734, the quasi-molecular ion of DPPC, is less intense and less contrasted than its fragments or those from SP-C, but reveals the same structure (Fig. 7 *Q*). At 30 mN/m domains cannot be imaged in the positive ion mode (Fig. 7, *B*, *E*, *H*, *L*, *O*, and *R*); however, M26 and M42 make slight contrasts (not shown).

In the plateau region the distributions of M70, M110, M184, and M734 give a "network" of bright domains (Fig. 7, *F*, *M*, *P*, and *S*). M734 has a dim, but visible, contrast and that of M110 is marked despite a low overall intensity. Among the network, M110 is distributed inhomogeneously, displaying several bright patches that are not expressed that clearly in the other images. The distribution of M104 (Fig. 7 *I*) is inverse to that of M110 or M184, like at low pressure. Here in the plateau region contrast-enhancement was necessary to demonstrate this effect. M27 (Fig. 7 *C*) is distributed quite homogeneously, as other hydrocarbon ions are. The total intensity of M734 almost equals that of M110, but its contrast is poor.

Fig. 8 summarizes the images of the plateau obtained with different techniques. A sum image of several positive SI is shown in Fig. 8 *A* to illustrate the typical domain structure. It resembles the fluorescence (Fig. 8 *C*) as well as the low-resolution scanning force micrograph (Fig. 8 *D*). Other positive SI, like M30, M72, and M224, which are not shown here but are mentioned in the mass spectra section, yield similar images. In the negative ion mode the plateau domains are visualized by mapping the small fragments M26 and M42, of which only M42 is shown (Fig. 8 *B*). We obtain a distinctly heterogeneous distribution with high contrast, which corresponds to the TOF-SIMS analysis of positive SI, like M110 or M184, and to the fluorescence micrographs and scanning force micrographs.

DISCUSSION

The present paper is focused on a laterally resolved mass spectrometric analysis of supported lipid and lipid-peptide monolayers. Starting from binary lipid systems (DPPC/DPPG) and lipid-peptide mixtures (DPPC/SP-C and DPPG/SP-C) we investigated a ternary DPPC/DPPG/SP-C monolayer that is considered to mimic the alveolar lung surfactant. Our main purpose was to gain more insight into the chemical composition of the domain structures observed earlier by fluorescence microscopy, SFM, and very recently, also by scanning nearfield optical microscopy (SNOM) (Kramer et al., 2000).

Mass spectra

The mass spectrum of the ternary system contains fingerprint fragments in the mass range < 250 amu, which can be assigned to the polar headgroup of DPPC. These fragments

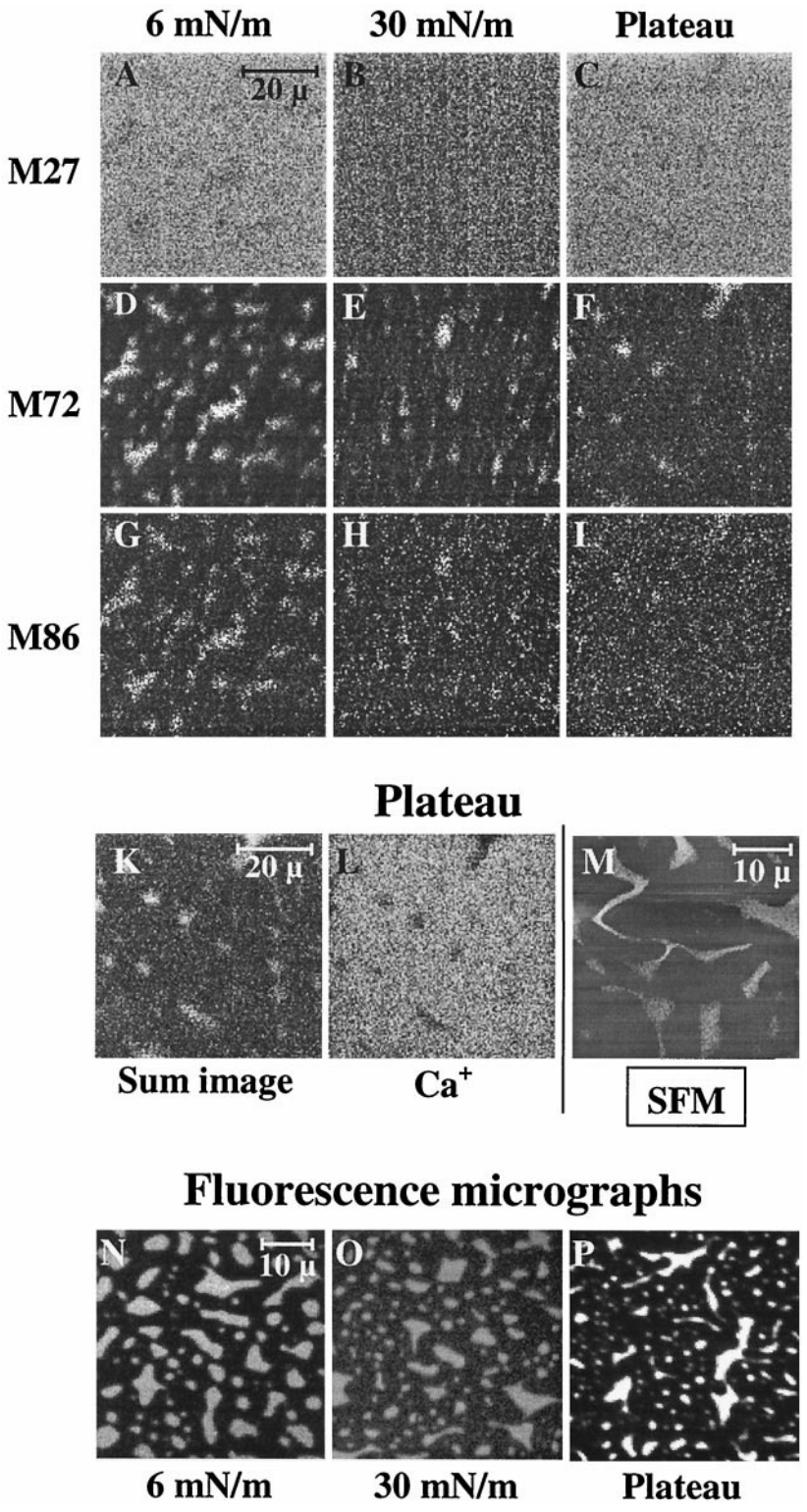

FIGURE 6 Images of DPPG/SP-C monolayers. (*A–I*) Maps of positive SI at 6, 30, and 50 mN/m (plateau); (*K*) Plateau, sum image of several amino acid-specific positive SI; (*L*) Plateau, Ca^+; PIDD: 1.9×10^{13} cm^{-2} (6 mN/m), 8.1×10^{12} cm^{-2} (30 mN/m), 5.9×10^{13} cm^{-2} (50 mN/m). (*M*) Plateau, scanning force micrograph. Bright areas are higher than the dark (no scale bar given). (*N–P*) Fluorescence micrographs at 6, 30, and 50 mN/m.

are also obtained by related techniques, such as FAB/MS (Ayanoglu et al., 1984; Matsuhara and Hayashi, 1991). In the molecular ion region, peaks similar to those obtained by MALDI (Harvey, 1995) are observed. DPPC is desorbed both as protonated and dehydrogenated quasi-molecular ion $(DPPC \pm H)^+$. ^{252}Cf plasma desorption MS (Demirev, 1987) exhibits similar results in the fingerprint range. DPPG is found negatively charged, which is not shown here; the protonated phosphoglycerol residue M173 is the only positive SI characteristic for DPPG (in spectra of spin-coated

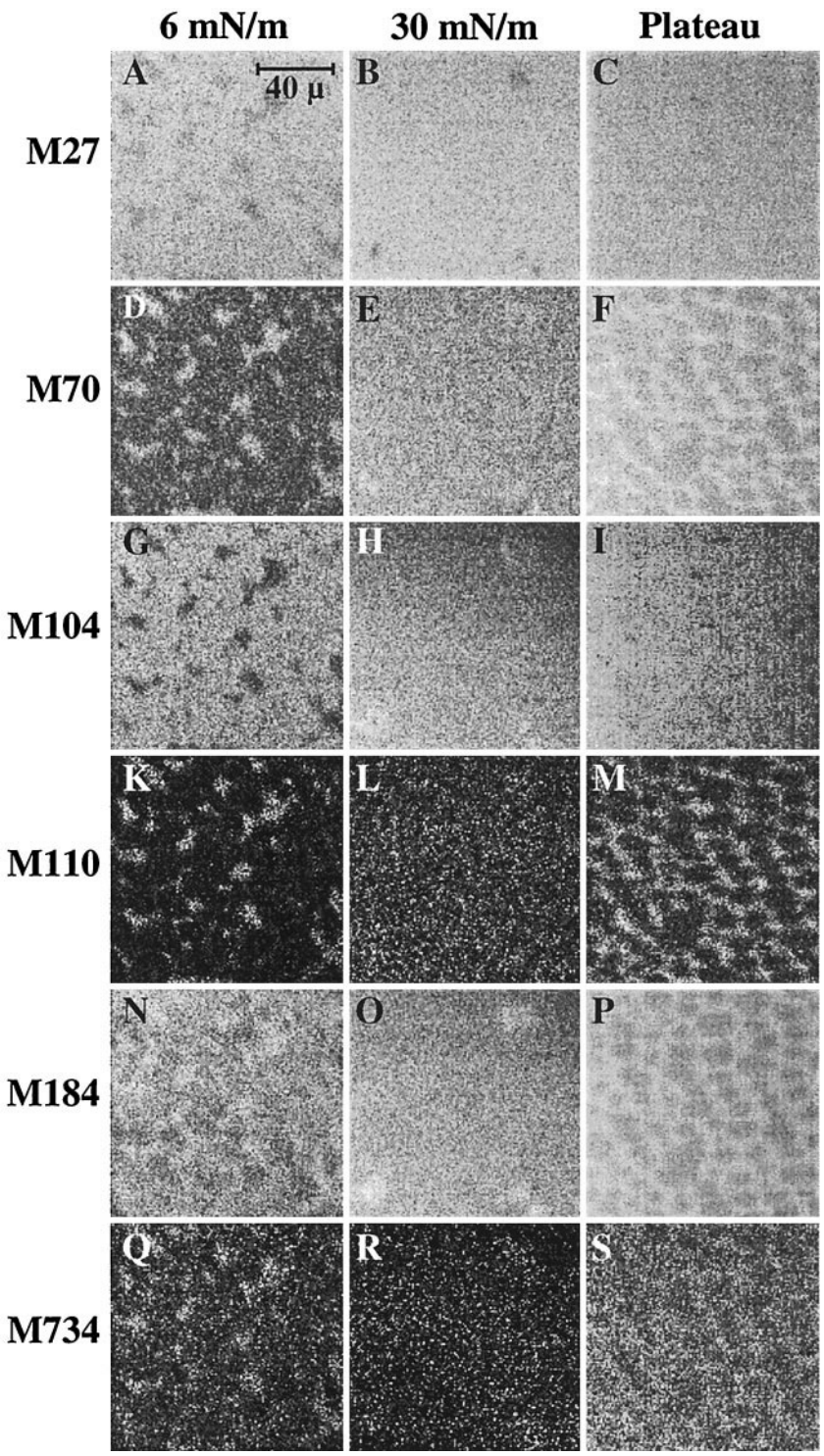

FIGURE 7 Images of layers prepared from the ternary mixture DPPC/DPPG/SP-C. (*A–S*) Maps of positive SI at 6, 30, and 50 mN/m; (*G*) is digitally enhanced. PIDD 8.1×10^{12} cm^{-2} (6 mN/m), 2.0×10^{13} cm^{-2} (30 mN/m), 4.6×10^{13} cm^{-2} (50 mN/m).

DPPG, a sodiated quasi-molecular ion (DPPG + 2Na − $H)^+$ could be detected in the positive ion mode). Because DPPC and DPPG differ in their headgroup, the mass range < 200 amu can be used for the identification of DPPC: M104, M166, and M184, as well as other fragments listed in the table, are typical of DPPC but are not included in the DPPG spectrum. Other typical phospholipid fragments are not discussed here because they do not yield additional information.

The SP-C spectrum consists of pronounced amino acid peaks $(M\text{-}45)^+$ (Hagenhoff, 1993), arising from a net cleavage of the $COOH^-$-group. Fragments of the basic residues,

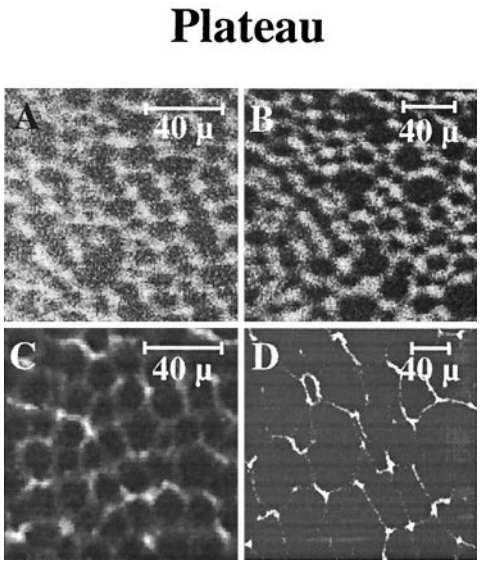

FIGURE 8 Additional images from the plateau region of DPPC/DPPG/SP-C layers: (*A*) Sum image of several positive SI; (*B*) M42 (CNO^-); (*C*) Fluorescence micrograph; (*D*) Scanning force micrograph.

$(Lys\text{-}45)^+$ and $(Arg\text{-}45)^+$, corresponding to M101 and M129, respectively, are not found; because of their unpaired electron they are only expected to emerge with very small intensity according to the nitrogen rule (McLafferty and Turecek, 1993). The small fragments M30 and M44 do not only originate from glycine and alanine, respectively, but are general constituents of peptide mass spectra (McLafferty and Turecek, 1993).

Most of the nitrogen-containing SI in the mass range $<$ 100 amu interfere with non-specific hydrocarbon SI, recognized by asymmetrically shaped peaks. In fact, this does not matter much, because the intense nitrogen-containing SI (with paired electrons) have even nominal masses, whereas the intense hydrocarbon ions have odd masses or odd numbers of hydrogen atoms, respectively. So an intense N-containing fragment interferes with a less intense hydrocarbon, and vice versa. For instance, at nominal mass 70 $C_4H_8N^+$ interferes with $^{13}CC_4H_9^+$ and $C_5H_{10}^+$. The latter peak is small, because it has an unpaired electron. The contribution of the isotopomer ($^{13}CC_4H_9^+$) can be calculated from the lighter neighbored hydrocarbon SI ($C_5H_9^+$), taking into account the isotope distribution of carbon, where the portion of ^{13}C amounts to 1.1%. Thus ≈3% of the intensity of M70 are due to $^{13}CC_4H_9^+$ and 7% due to $C_5H_{10}^+$. So as a crude estimate we may assume a value of 10%, which is the "unspecific" share of a headgroup- or amino acid-based DPPC or SP-C peak. In fact, the intensity of the isotopomer increases with increasing C number.

In the negative ion spectra, which are not presented here, M42 is desorbed from SP-C more intensively than from DPPC (nearly 10-fold). The origin of M42 (CNO^-) can be attributed to the peptide bonds. A possible objection that M26 and M42 are ubiquitous impurities because of their smallness is invalidated by their insignificant yield in DPPG, which does not contain such a chemical group.

The SI yields in a single compound analysis, especially the yields of the quasi-molecular ions $(M + H)^+$, $(M +$ alkaline$)^+$, and $(M +$ metal$)^+$, depend on the method of deposition (spin coating, droplet preparation, or as LB film), on the substrate material, and on the pH. The deposition technique is crucial, because it is directly linked to the coverage of the substrate surface. When one deposits the same amount of a compound either as droplet or by spin-coating, the coverage is lower with the latter method. By LB preparation, the molecules can be deposited in a well-ordered state, and substrate-overlayer interactions are better-specified. For example, in the case of a hydrophilic transfer of DPPC onto gold it is known that the polar headgroup interacts directly with the substrate. For peptides, the presence of basic residues like arginine or lysine plays an important role in the desorption process (van Leyen et al., 1987). The fragmentation pattern of SP-C shown in Fig. 3 is characteristic, but SI intensities vary when applying different deposition techniques.

Ion images

The TOF-SIMS sum image of DPPC/DPPG at 6 mN/m corresponds well to the light microscopic picture of the silver-decorated sample: both differ from the FLM results, where the condensed domains are smaller (von Nahmen et al., 1997b). The reason for this may be the fact that the supported film is equilibrated before transfer, whereas a fluorescence micrograph is taken after halting the barrier of the film balance a few minutes, or during compression at very slow speed. Therefore, equilibration, which is necessary for an LB transfer, may cause a larger portion of the film being condensed as compared with a film at the air/water interface to a solid substrate and may result in a higher degree of condensation of an LB film, compared to its analog, at the air/water interface. At 30 mN/m, where the film is predominantly condensed, fluorescence micrographs show slight contrast (von Nahmen et al., 1997b), but with TOF-SIMS this contrast cannot be observed in the positive ion mode, not even by summing up and processing. In the negative ion mode a very dim contrast was observed when summing up some specific and unspecific SI and enhancing the contrast of the resulting image.

Correlating the TOF-SIMS results with those obtained by FLM (von Nahmen et al., 1997b) or SD, it is likely that the fluid phase, which is represented by the bright domains of both the silver and fluorescence contrast, corresponds to the bright domains in the maps of M58, M184, and M734, which are dark in the maps of M27 or Ca^+. The surface concentration of the parental molecules is lower, but the intensity of M58, for example, is higher in the fluid than in the condensed phase. Because we already know that DPPC

and DPPG mix nearly ideally at a 4:1 molar ratio (Garidel et al., 1997; Sieber, unpublished x-ray reflection data), a pronounced matrix effect must account for the different SI intensities or ionization rates in the fluid and condensed phase. Although the SI spectrum of DPPG does not engender any specific fragments, DPPG could be mapped only due to the contrast generated by the DPPC-specific SI. Thus the ion images arise from a physical contrast due to co-existing phases, like in one- or two-component LB films studied earlier (Bourdos et al., 2000; Leufgen et al., 1996).

In the DPPC/DPPG/SP-C film, results are similar at 6 and 30 mN/m. At 6 mN/m, the fluid domains are smaller and the domain structure is more disrupted than in the corresponding binary lipid film. At 30 mN/m again there is no contrast. As in the DPPC/DPPG film, FLM and TOF-SIMS results do not correspond exactly, for the reasons given above. However, in addition to the mere physical contrast, a chemical contrast is superposed because there is SP-C present in the mixture, which can be distinguished from the lipids by certain amino acid fragments, but superposition of two contrasts complicates the interpretation. By looking at the lipid fragments at 6 mN/m, we could assume the existence of co-existing phases, as for the DPPC/DPPG film, although a possible electrostatic interaction between DPPG and SP-C may cause a certain degree of demixing. The choline ion M104 is worth considering because its contrast is opposite to M184 or M734, with higher intensity in the condensed than in the fluid phase, comparable to M27 and Ca^+ (not shown for the ternary system). The distribution of the highly SP-C-specific M110 may mislead: one is tempted to see the SP-C strictly localized in the bright domains, sustained by the fact that on the one hand SP-C makes up only 0.4% of the mixture, but on the other hand its fragments are desorbed intensely from the fluid domains; this may, however, be distorted by a matrix effect. For a fairly good interpretation it is therefore always necessary to *correlate* the TOF-SIMS maps with other imaging techniques. Considering earlier findings obtained with FLM (Nag et al., 1996; von Nahmen et al., 1997b), we can conclude that the amino acid-specific fragments like M110 give a correct image of the distribution of SP-C in lipid monolayers, i.e., the peptide is associated with the fluid phase.

The lateral distribution of SP-C in a single phospholipid matrix is quite different for DPPC and DPPG. In DPPC/SP-C there is no contrast observed at both low and high pressure in the distribution of all ions we considered and, of which we show only two, representative of DPPC- and SP-C. This indicates full miscibility of SP-C and DPPC in correspondence with microfluorescence measurements (von Nahmen, 1997). The pressure drop in the plateau upon halting the barrier of the film balance is due to a loss of material. Interaction of DPPC with 0.5 mol % SP-C alone obviously cannot accomplish the formation of a stable collapse structure.

However, domains are observed in DPPG/SP-C at each of the considered film pressures. As in the ternary system, SP-C induces a plateau at high pressure ($>$50 mN/m) which, upon halting barriers, settles to an equilibrium, indicating a stable collapse state that allows an LB transfer. This points at a pronounced electrostatic interaction between the negatively charged DPPG and SP-C, which carries positive charges at its basic residues. Because the isotherm shows no demixing, the SI images at least illustrate the formation of separated phases. At higher pressures the contrast vanishes due to continual condensation, comparable to the DPPC/DPPG system; therefore, the fluorescence micrographs are not easy to compare with the ion images, although there is a good agreement at 6 mN/m and in the plateau with respect to the sum image. In the plateau region, the fluorescence intensity gets brighter in the fluid domains due to higher concentration of the probe molecules (NBD-PG) per unit area. This is interpreted by the formation of three-dimensional multilayer stacks (Galla et al., 1998). Stack formation was assumed earlier from ellipsometric measurements (Post et al., 1995) and confirmed here by imaging the topography with SFM (Amrein et al., 1997). Here we observed that the (bright) areas of elevated height in the SFM pictures correspond to the bright domains of the sum image of amino acid SI and in the fluorescence image. From our TOF-SIMS or FLM images alone we may not conclude that SP-C is enriched in the multilamellar domains for two reasons: 1) TOF-SIMS images are impaired by a matrix effect, and 2) in the FLM measurements presented here no dye-labeled SP-C is used, but labeled DPPG is. However, NBD-labeled SP-C was applied earlier with the ternary mixture used here by von Nahmen et al. (1997b), yielding similar results to a film containing NBD-PC. The use of dye-labeled SP-C gave a clearer hint that SP-C is enriched in the stacks. It has to be stated that from the TOF-SIMS measurements alone the existence of multilayer domains cannot be derived. The capabilities of TOF-SIMS are limited in this respect because of its extreme surface sensitivity, depending also on the nature of the primary ion beam (Kötter and Benninghoven, 1998). The more distant a molecule is located to the substrate, the less it will be affected by the sputter event initiated by the collision cascade among the substrate molecules, so multilayers normally come to reduced SI yields, as shown by Stapel et al. (1999). Moreover, quantities that describe the phenomenology of SI formation, like the disappearance cross-section, are only defined for monolayers.

With respect to the Ca^+-image one should recall that *intrinsic* ions are detected with TOF-SIMS; they only amount to $\approx$1% of the desorbed particles, the rest of which are neutrals. The mechanisms of ion formation, fragmentation, and desorption from organic molecules adsorbed to solids are not fully understood, which applies even more to overlayers like LB films. Ca^+, in contrast, is not to the same extent affected by matrix effects like organic fragments,

because it does not arise from complex ionization mechanisms rather than simple ionization. This applies especially to alkaline or alkaline-earth elements with low ionization energies. We therefore think that the Ca^+ map nearly reflects the distribution of Ca^+ at the surface.

The plateau of DPPC/DPPG/SP-C

Both DPPC-specific (M184, M734) and SP-C-specific (M70, M110, the negative M42) fragments yield the same network-like domain structure, best visible in the sum image of some positive SI. Identical structures were also obtained with FLM or low-resolution SFM (von Nahmen et al., 1997a, b). The SFM images arise from a topographic contrast due to distinct protrusions, which form when the model surfactant film partially collapses (Amrein et al., 1997). The protrusions are supposed to be the surfactant reservoir, probably multilamellar stacks from which the excluded material is reinserted into the monolayer when the film is expanded. From fluorescence data and from SFM pictures these stacks are assumed to consist of an odd number of layers.

However, high-resolution images exhibit no continuous formation of protrusions, rather than the existence of small patches (von Nahmen et al., 1997a). From this we conclude that the fluid "network" includes the adjacent intermediate monolayer domain, and is not only a network of layered lamellae. The similar network-like distribution of SP-C-specific SI, like M110, indicates that SP-C is present throughout the network, and not only in the postulated stacks. It seems to be kept as spare material, which is supplied for the formation of more stacks upon further compression. This is consistent with SFM images taken at successive points in the plateau region during compression, where the proportion of protruded areas increases with decreasing molecular area. In FLM measurements on the ternary system using fluorescence-labeled SP-C and PC, the fluorescence intensity increased in those areas related to the postulated stacks. As in DPPG/SP-C, this is due to a volume effect where flat monolayers escape into the third dimension in agreement with the squeeze-out hypothesis by Bangham (1979); DPPC, however, as it is demonstrated here by the distribution of M184, seems to be located in these domains in considerable amounts, too. This would contradict Bangham's hypothesis, stating that upon film collapse only non-DPPC components are excluded from the monolayer and pure, condensed DPPC should remain at the interface, maintaining low surface tension.

Upon scrutinizing the TOF-SIMS results obtained from the plateau region, one has to consider the above-mentioned volume effect, which normally brings about lower SI intensities from multilayers, although a higher local concentration of the parental molecule is possible due to layering (an effect being less pronounced when multi-atomic or noble gas PI sources are used, as shown by Stapel et al., 1999). Therefore it is crucial to know to what extent both effects compensate each other. Moreover, as discussed above, a matrix effect becomes even more complicated if different physical states are involved in the SI formation. All together, these effects make it impossible to determine whether SP-C is really squeezed out of the condensed monolayer phase, but intensities of many DPPC- and SP-C-based fragments are higher in the network than in the "patches." Because the network is supposed to contain the layered part of the film, thus being subject to the volume effect, one expects lower yields in it. Thus we claim that the major share of the SP-C content is located in the network, which corresponds very well with the FLM results. Because the existence of multilayers would reduce SI intensities, the discrepancy between intensity and concentration is even increased. For the assessment of the distribution of DPPC the FLM micrographs are not helpful, as they are for the distribution of SP-C. SP-C could be replaced completely by a fluorescent analog, whereas this is not possible for DPPC, the major component of the surfactant.

A completely different behavior was observed with M27, a hydrocarbon SI, that is distributed more homogeneously in the plateau than other either DPPC- or SP-C-based SI. Hydrocarbon ions neither seem to be affected that strongly by multilayer formation nor by lateral pressure, i.e., the physical state of the film. The latter corresponds to the fact that hydrocarbon ions mainly originate from the acyl chains (Bourdos et al., 2000), of which especially the methyl and ethyl endgroups are less sensitive to changes of the lateral pressure. M104 again exhibits contrast inverse to various other SI, although not as pronounced as at 6 mN/m, where it was shown that this SI is more intense in the fluid phase. Its intensity in the plateau may be lowered by both the existence of multilayers and a possible higher fluidity of the network.

CONCLUSION

We used TOF-SIMS to visualize chemically and physically different domain structures in mixed LB films of phospholipids and phospholipids with SP-C, with particular interest in the ternary system DPPC/DPPG/SP-C. For the collapsed ternary film we showed in accordance with previous work that upon compression of the monolayer a network-like SP-C-rich structure—the surfactant reservoir—is formed, which comprises an intermediate, also SP-C-enriched, monolayer phase. Correlation of FLM and TOF-SIMS data allows the conclusion that the major share of the SP-C molecules is located in the network. The squeeze-out hypothesis that only non-DPPC components leave the monolayer could not be verified. Despite the unclear matrix effect, especially in the presence of multilayers, we are allowed to assume that a considerable amount of DPPC remains in the protrusions, contradicting one aspect of this hypothesis but confirming its basic idea. Within the dis-

cussed limitations, TOF-SIMS turns out to be a valuable tool for studying biological model systems. For interpreting the lung surfactant it is important to keep in mind that the simple mixture of disaturated phospholipids of course does not exhibit the richness of biophysical activity of native surfactant. Our aim was to elucidate the role of the SP-C in forming and stabilizing the surfactant reservoir.

We thank Detlef Knebel (Institut für Medizinische Physik und Biophysik, Universität Münster) for the SFM image of DPPG/SP-C, and Michael Gleiche (Physikalisches Institut, Universität Münster), who assisted in preparing the silver-decorated samples and acquiring the images.

This work was supported by Grant GA 233/18-1 from the Deutsche Forschungsgemeinschaft.

REFERENCES

Amrein, M., A. von Nahmen, and M. Sieber. 1997. A scanning force- and fluorescence light microscopy study of the structure and function of a model pulmonary surfactant. *Eur. Biophys. J.* 26:349–357.

Ayanoglu, E., A. Wegmann, O. Pilet, G. D. Marbury, J. R. Hass, and C. Djerassi. 1984. Mass spectrometry of phospholipids. Some applications of desorption chemical ionization and fast atom bombardment. *J. Am. Chem. Soc.* 106:5246–5251.

Bangham, A. D. 1979. The physical properties of an effective lung surfactant. *Biochim. Biophys. Acta.* 573:552–556.

Benninghoven, A. 1994. Chemical analysis of inorganic and organic surfaces and thin films by static time-of-flight secondary ion mass spectrometry (TOF-SIMS). *Angew. Chem. Int. Ed. Engl.* 33:1023–1044.

Benninghoven, A., B. Hagenhoff, and E. Niehues. 1993. Surface MS: probing real-world samples. *Anal. Chem.* 65: 630A–640A.

Bertrand, P., and L. Weng. 1996. Time-of-flight secondary ion mass spectrometry (ToF-SIMS). *Mikrochim. Acta.* 13:167–182.

Bourdos, N., F. Kollmer, A. Benninghoven, M. Sieber, and H.-J. Galla. 2000. Imaging of domain structures in a one-component lipid monolayer by time-of-flight secondary ion mass spectrometry. *Langmuir.* 16: 1481–1484.

Clements, J. A. 1962. Surface phenomena in relation to pulmonary function. *Physiologist.* 5:11–28.

Cochrane, C. G., and S. D. Revak. 1991. Pulmonary surfactant protein B (SP-B): structure-function relationships. *Science.* 254:566–568.

Demirev, P. A. 1987. 252-Californium plasma desorption mass spectrometry of glycerophospholipids. *Biomed. Environ. Mass Spectrom.* 14: 241–246.

Discher, B. M., K. M. Maloney, W. R. Schief, V. Vogel, and S. B. Hall. 1996. Lateral phase separation in interfacial films of pulmonary surfactant. *Biophys. J.* 71:2583–2590.

Galla, H.-J., N. Bourdos, A. von Nahmen, M. Amrein, and M. Sieber. 1998. The role of pulmonary surfactant protein C during the breathing cycle. *Thin Solid Films.* 329:632–635.

Garidel, P., C. Johann, L. Mennicke, and A. Blume. 1997. The mixing behaviour of pseudobinary phosphatidylcholine-phosphatidylglycerol mixtures as a function of pH and chain length. *Eur. Biophys. J.* 26: 447–459.

Gleiche, M., L. F. Chi, and H. Fuchs. 1998. Molecular property related silver decoration on fatty acid Langmuir-Blodgett monolayers. *Thin Solid Films.* 329:268–272.

Hagenhoff, B. 1993. Sekundärionenmassenspektrometrie an Molekularen Oberflächenstrukturen. Ph.D. thesis. Westfälische Wilhelms-Universität, Münster. 178 pp.

Hagenhoff, B. 1995. Surface mass spectrometry: application to biosensor characterization. *Biosensors and Bioelectronics.* 10:885–894.

Hagenhoff, B., A. Benninghoven, J. Spinke, M. Liley, and W. Knoll. 1993. Time-of-flight secondary ion mass spectrometry investigations of self-assembled monolayers of organic thiols, sulfides, and disulfides on gold surfaces. *Langmuir.* 9:1622–1624.

Harvey, D. J. 1995. Matrix-assisted laser desorption/ionization mass spectrometry of phospholipids. *J. Mass Spectrom.* 30:1333–1346.

Harwood, J. L. 1987. Lung surfactant. *Prog. Lipid. Res.* 26:211–256.

Horowitz, A. D., B. Elledge, J. A. Whitsett, and J. E. Baatz. 1992. Effects of lung surfactant proteolipid SP-C on the organization of model membrane lipids: a fluorescence study. *Biochim. Biophys. Acta.* 1107:44–54.

Johansson, J., and T. Curstedt. 1997. Molecular structures and interactions of pulmonary surfactant components. *Eur. J. Biochem.* 244:675–693.

Johansson, J., T. Curstedt, and B. Robertson. 1994a. The proteins of the surfactant system. *Eur. Respir. J.* 7:372–391.

Johansson, J., T. Szyperski, T. Curstedt, and K. Wüthrich. 1994b. The NMR structure of the pulmonary surfactant-associated polypeptide SP-C in an apolar solvent contains a valyl-rich a-helix. *Biochemistry.* 33: 6015–6023.

King, R. J., and J. A. Clements. 1972. Surface active material from dog lung. I. Method of isolation. *Am. J. Physiol.* 223:715–726.

Kötter, F., and A. Benninghoven. 1998. Secondary ion emission from polymer surfaces under Ar, Xe and SF_5 ion bombardment. *Appl. Surf. Sci.* 133:47–57.

Kramer, A., A. Wintergalen, M. Sieber, H. J. Galla, M. Amrein, and R. Guckenberger. 2000. Distribution of the surfactant associated protein C within a lung surfactant model film investigated by near-field optical microscopy. *Biophys. J.* 78:454–465.

Krüger, P., M. Schalke, Z. Wang, R. H. Notter, R. A. Dluhy, and M. Lösche. 1999. Effect of hydrophobic surfactant peptides SP-B and SP-C on binary phospholipid monolayers. I. Fluorescence and dark-field microscopy. *Biophys. J.* 77:903–914.

Leufgen, K. M., H. Rulle, A. Benninghoven, M. Sieber, and H-J. Galla. 1996. Imaging time-of-flight secondary ion mass spectrometry allows visualization and analysis of coexisting phases in Langmuir-Blodgett films. *Langmuir.* 12:1708–1711.

Liu, M. 1997. Synchronized changing of transinterface pressure, bubble radius and surface tension: a unique feature of lung surfactant. *Chem. Phys. Lipids.* 89:55–65.

Matsuhara, T., and A. Hayashi. 1991. FAB/Mass spectrometry of lipids. *Prog. Lipid Res.* 30:301–322.

McLafferty, F. W., and F. Turecek. 1993. Interpretation of Mass Spectra. University Science Books, Mill Valley, CA.

Nag, K., J. Pèrez-Gil, A. Cruz, and K. M. W. Keough. 1996. Fluorescently labeled pulmonary surfactant protein C in spread phospholipid monolayers. *Biophys. J.* 71:246–256.

Nag, K., S. G. Taneva, J. Pèrez-Gil, A. Cruz, and K. M. W. Keough. 1997. Combinations of fluorescently labeled pulmonary surfactant proteins SP-B and SP-C in phospholipid films. *Biophys. J.* 72:2638–2650.

Oosterlaken-Dijksterhuis, M. A., H. P. Haagsman, L. M. G. van Golde, and R. A. Demel. 1991a. Interaction of lipid vesicles with monomolecular layers containing lung surfactant proteins SP-B or SP-C. *Biochemistry.* 30:8276–8281.

Oosterlaken-Dijksterhuis, M. A., H. P. Haagsman, L. M. G. van Golde, and R. A. Demel. 1991b. Characterization of lipid insertion into monomolecular layers mediated by lung surfactant proteins SP-B and SP-C. *Biochemistry.* 30:10965–10971.

Panaiotov, I., Tz. Ivanova, J. Proust, F. Boury, B. Denizot, K. Keough, and S. Taneva. 1996. Effect of hydrophobic protein SP-C on structure and dilatational properties of the model monolayers of pulmonary surfactant. *Colloids Surf. B: Biointerfaces.* 6:243–260.

Pèrez-Gil, J., K. Nag, S. Taneva, and K. M. W. Keough. 1992a. Pulmonary surfactant protein SP-C causes packing rearrangements of dipalmitoylphosphatidylcholine in spread monolayers. *Biophys. J.* 63:197–204.

Pèrez-Gil, J., J. Tucker, G. Simatos, and K. M. W. Keough. 1992b. Interfacial adsorption of simple lipid mixtures combined with hydrophobic surfactant protein from pig lung. *Biochem. Cell Biol.* 70:332–338.

Post, A., A. von Nahmen, M. Schmitt, J. Ruths, H. Riegler, M. Sieber, and H-J. Galla. 1995. Pulmonary surfactant protein C containing lipid films at the air-water interface as a model for the surface of lung alveoli. *Mol. Membr. Biol.* 12:93–99.

Rulle, H. 1996. Hochauflösende Abbildungen Strukturiertet Organischer Oberflächen mit Flugzeit-sekundärionen-Massenspektrometrie (TOF-SIMS). Ph.D. thesis. Westfälische Wilhelms-Universität, Münster. 88 pp.

Scarpelli, E. M., and A. J. Mautone. 1994. Surface biophysics of the surface monolayer theory is incompatible with regional lung function. *Biophys. J.* 67:1080–1089.

Schürch, S., J. Goerke, and J. A. Clements. 1976. Direct determination of surface tension in the lung. *Proc. Natl. Acad. Sci. U.S.A.* 73:4698–4702.

Schürch, S., R. Qanbar, H. Bachofen, and F. Possmeyer. 1995. The surface-associated surfactant reservoir in the alveolar lining. *Biol. Neonate.* 67(Suppl. 1):61–76.

Schwieters, J., H. G. Cramer, T. Heller, U. Juergens, E. Niehuis, J. Zehnpfennig, and A. Benninghoven. 1991. High mass resolution surface imaging with a time-of-flight secondary ion mass spectroscopy scanning microprobe. *J. Vac. Sci. Technol. A.* 9:2864–2871.

Sen, A., S.-W. Hui, M. Mosgrober-Anthony, B. A. Holm, and E. A. Egan. 1988. Localization of lipid exchange sites between bulk lung surfactants and surface monolayer: freeze fracture study. *J. Colloid Interface Sci.* 126:355–360.

Shelly, S. A., J. E. Paciga, and J. U. Balius. 1984. Lung surfactant phospholipids in different animal species. *Lipids.* 19:857–862.

Stapel, D., O. Brox, and A. Benninghoven. 1999. Secondary ion emission from arachidic acid LB-layers under Ar, Xe, Ga and SF_5 primary ion bombardment. *Appl. Surf. Sci.* 140:156–167.

Taneva, S. G., and K. M. W. Keough. 1994a. Dynamic surface properties of pulmonary surfactant proteins SP-B and SP-C and their mixtures with dipalmitoylphosphatidylcholine. *Biochemistry.* 33:14660–14670.

Taneva, S. G., and K. M. W. Keough. 1994b. Pulmonary surfactant proteins SP-B and SP-C in spread monolayers at the air-water interface: I. Monolayers of pulmonary surfactant protein SP-B and phospholipids. *Biophys. J.* 66:1137–1148.

Taneva, S. G., and K. M. W. Keough. 1994c. Pulmonary surfactant proteins SP-B and SP-C in spread monolayers at the air-water interface: II. Monolayers of pulmonary surfactant protein Protein SP-C and phospholipids. *Biophys. J.* 66:1149–1157.

Taneva, S. G., and K. M. W. Keough. 1994d. Pulmonary surfactant proteins SP-B and SP-C in spread monolayers at the air-water interface: III. Proteins SP-B plus SP-C with phospholipids in spread monolayers. *Biophys. J.* 66:1158–1166.

Tchoreloff, P., A. Gulik, B. Denizot, J. E. Proust, and F. Puisieux. 1991. A structural study of interfacial phospholipid and lung surfactant layers by transmission electron microscopy after Blodgett sampling: influence of surface pressure and temperature. *Chem. Phys. Lipids.* 59:151–165.

van Leyen, D., D. Greifendorf, and A. Benninghoven. 1987. Secondary ion formation from peptides: influence of primary structure and substrates. 6th International Conference on Secondary Ion Mass Spectrometry, Versailles, Sept. 13–18, 679–682.

von Nahmen, A. 1997. Strukturelle Organisation von Surfactant Protein C haltigen Phospholipid-Monoschichten an der Luft-Wasser-Grenzfläche—Ein Modell des alveolären Surfactant. Ph.D. thesis. Westfälische Wilhelms-Universität, Münster. 139 pp.

von Nahmen, A., A. Post, H. J. Galla, and M. Sieber. 1997b. The phase behaviour of lipid monolayers containing pulmonary surfactant protein C studied by fluorescence light microscopy. *Eur. Biophys. J.* 26: 359–369.

von Nahmen, A., M. Schenk, M. Sieber, and M. Amrein. 1997a. The structure of a model pulmonary surfactant as revealed by scanning force microscopy. *Biophys. J.* 72:463–469.

Wang, Z., O. Gurel, J. E. Baatz, and R. H. Notter. 1996b. Differential activity and lack of synergy of lung surfactant proteins SP-B and SP-C in interactions with phospholipids. *J. Lipid Res.* 37:1749–1760.

Wang, Z., S. B. Hall, and R. H. Notter. 1995. Dynamic surface activity of films of lung surfactant phospholipids, hydrophobic proteins, and neutral lipids. *J. Lipid Res.* 36:1283–1293.

Wang, Z., S. B. Hall, and R. H. Notter. 1996a. Roles of different hydrophobic constituents in the adsorption of pulmonary surfactant. *J. Lipid Res.* 37:790–798.